CRYSTAL GROWTH & DESIGN

Article

Cite This: Cryst. Growth Des. 2017, 17, 5823-5837

pubs.acs.org/crystal

Probability of Nucleation in a Metastable Zone: Cooling Crystallization and Polythermal Method

Venkateswarlu Bhamidi,*[,†] Paul J. A. Kenis,[‡] and Charles F. Zukoski[§]

[†]Scale-up and Process Innovation, Eastman Chemical Company, 200 South Wilcox Drive, Kingsport, Tennessee 37662, United States

[‡]Chemical & Biomolecular Engineering, University of Illinois at Urbana−Champaign, 600 South Mathews Avenue, Urbana, Illinois 61801, United States

[§]Chemical and Biological Engineering, University at Buffalo, The State University of New York, 310 Fumas Hall, Buffalo, New York 14260, United States

Supporting Information

ABSTRACT: In polythermal experiments, typically the observed dependence of the metastable zone width (MZW − often characterized as the undercooling ΔT) on the experimental path is attributed to the variation of the nucleation rate of solute crystals along this path. In this work, we analyze the experimental data on the MZW for several solutes available in the literature and show that the path-dependence of MZW observed during this cooling crystallization may not always exist when one considers the supersaturation of nucleation. This result is in line with our previous observations on the MZW of various other solutes exhibited during evaporative crystallization. In this context, the assumptions behind the traditional theoretical explanations of MZW are examined, and the possible issues in obtaining nucleation kinetics from polythermal MZW experiments are discussed. A consistent method for determining the nucleation rate parameters, which leverages the complementary nature of both the induction time (IT) and the MZW experiments, is proposed. This work aims to bring the often-overlooked fundamental variables of crystal nucleation into the forefront of the analysis of polythermal experiments.

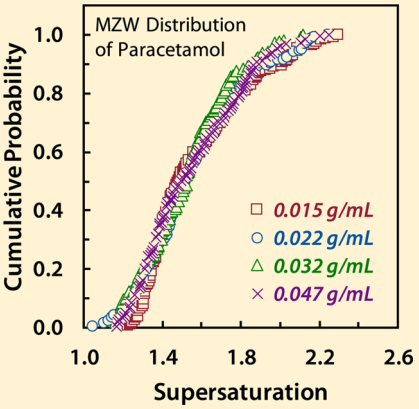

1. INTRODUCTION

Because of its importance in several areas of science and technology,[1−3] and as an industrial purification process,[4] solution crystallization is of significant interest to researchers. Intriguingly, crystallizing systems often endure significant metastability, and typically crystals do not nucleate in a solution until the system crosses a metastable region on the phase diagram.[5] The extent of this region for a given solute is often characterized experimentally through the determination of a metastable zone width (MZW). Knowledge of how this MZW varies with solution conditions is considered to offer an important guideline in the design and operation of industrial crystallizers.[4,6] Crystal nucleation is driven by a change in the chemical potential of a solute, $\Delta\mu$, which is expressed through the supersaturation, S. Thus, the metastable zone width characterizes essentially the supersaturation of nucleation, S_n, exhibited by a solute when it is continuously driven toward a phase transformation.

The metastable zone (MZ) of a solute is frequently explored through experiments that gradually cool a solution that contains a fixed amount of solute (the "polythermal" method).[7] In this method, the temperature of crystal nucleation, T_n, is determined during a *continuous* cooling of the solution at a fixed cooling rate. The MZW is then characterized in terms of the degree of undercooling ΔT sustained by the solution before nucleation is observed. This ΔT is typically defined as the difference between the saturation and the nucleation temperatures, T_{sat} and T_n, respectively (i.e., $\Delta T = T_{sat} - T_n$). Polythermal experiments consistently show that greater rates of cooling result in larger values of ΔT.[8,9] These observations suggest that the MZW must be a kinetic phenomenon controlled by the path of the experiment, i.e., the evolution of supersaturation during the experiment. From this perspective, many theoretical/semi-empirical approaches were developed over the last several decades to predict ΔT as a deterministic quantity.[10−15] More rigorous stochastic models have considered the inherent probabilistic nature of crystal formation.[16−20] Both these deterministic and stochastic approaches describe the MZW for a system as a limit controlled by the path-dependent rate of nucleation. In other words, within the scope of these models, one can define an S_n only with reference to the experimental path and the supersaturation dependence of the rate of nucleation.

Recently, using a microfluidic crystallization platform, we studied the supersaturation of nucleation exhibited by a broad class of compounds during slow evaporation of solvent.[21] The probability distribution of S_n observed in these experiments could not be explained using the traditional theoretical descriptions that consider a time-varying nucleation rate. The experimental results indicated that when a system is super-

Received: June 21, 2017
Revised: September 5, 2017
Published: October 20, 2017

DOI: 10.1021/acs.cgd.7b00875
Cryst. Growth Des. 2017, 17, 5823−5837

saturated sufficiently slowly, the probability distribution of MZWs exhibited by that system approaches a "limiting distribution" that becomes path-independent. This limiting MZW distribution is solely governed by the variation of the energy barrier during the experiment.[21] The key outcome of this work was the realization that the metastable zone width is a kinetic phenomenon due only to the time lag involved in the equilibration of the system to the changing experimental conditions and not because of a steady-state (i.e., equilibrated) rate of nucleation that varies along the path. The path-dependence of MZW predicted by the widely used steady-state nucleation rate models is an artifact of the assumptions employed in the model development.

Present work builds on our earlier observations with evaporative crystallization. The objectives of the present work are two-fold. First, we demonstrate the applicability of the new thought process to the analysis of MZW experiments that use cooling crystallization. The key difference between the evaporative (isothermal) and cooling (polythermal) crystallizations is that in the former the solubility of the solute remains constant during the experiment, whereas in the latter it varies. This work thus examines the validity of the recently developed concepts about the origins of the metastable zone to the case of time-varying solubility. Second, we discuss the unsuitability of MZW experiments to obtain the supersaturation dependence of the steady-state nucleation rate for a solute. Here we consider two possible scenarios of determining the MZW in polythermal experiments: (i) from experiments that use solutions of different compositions, but use the same cooling rate, and (ii) from experiments conducted with various cooling rates using solutions with fixed composition. We analyze the experimental results available in the literature for several solutes by treating the MZW as a path-independent stochastic variable. The crystal nucleation rate parameters for a solute obtained from both induction time (IT) experiments and MZW experiments are compared and the inconsistencies are highlighted. The discussion is concluded with a focus on the complementary nature of the IT and MZW experiments in providing the nucleation kinetics information.

2. STOCHASTIC ANALYSIS OF NUCLEATION

2.1. Conventional Approach. The stochastic analysis of a nucleation experiment is typically carried out by considering the time of nucleation in a system. Nucleation is inherently a *discrete* process that results in the formation of individual crystals. To enable a *time-continuous* description of nucleation, one first *assumes* that the probability of nucleation in any infinitesimal time interval dt varies linearly with a rate κ. In other words, the change in the probability of nucleation within a time interval $(t, t + dt)$ is assumed to be given by κdt.

2.1.1. Nucleation at Constant Supersaturation. For a system nucleating at a constant supersaturation S, the cumulative probability $F(t)$ of finding at least one nucleus (crystal) at a time t after the system has equilibrated to S may be derived in terms of κ as[17,21,22]

$$F(t) = 1 - e^{-\kappa t} \tag{1}$$

The time that corresponds to the mean of the probability distribution represented by eq 1 is given by

$$t_{mean} = \int_0^\infty t\, \kappa\, e^{-\kappa t}\, dt = 1/\kappa \tag{2}$$

This mean time is often referred to as the *induction time* of nucleation, τ, for the solute at S. The inverse of this induction time, κ, which originally was defined as the rate of change of *transition* probability (the probability that a system transitions from having no nuclei to having a single nucleus), may be interpreted as the mean rate at which the system generates nuclei. Equation 1 thus provides one a *working definition* of nucleation rate in the *entire system* in the stochastic sense. This model of nucleation probability is often referred to as the Poisson model due to its prediction of nucleation probability density $f(t) = dF(t)/dt$ to decay exponentially in a memoryless manner.[23]

Note that the above Poisson approach is founded on one crucial *assumption*: the transition probability of nucleation varies *linearly at a constant rate* κ in any infinitesimal time interval $(t, t + dt)$. Thus, the nucleation rate, in its stochastic sense, is merely a hypothesis introduced to facilitate a time-continuous description of an inherently discrete process of nucleation. This hypothesis allows one to rationalize the observed randomness in the time of formation of the first crystal (t_n) at a fixed supersaturation. By fitting the experimental data on the cumulative distribution of t_n to eq 1, one obtains this hypothetical "nucleation rate" κ without any need for further theoretical considerations. This κ may *later* be associated with the steady-state nucleation rate J provided by the classical nucleation theory (CNT) by interpreting $\kappa = JV$, where V is the volume of the solution.[22,24]

2.1.2. Nucleation with Variable Supersaturation. The analysis of a *metastable zone* experiment is conventionally carried out by a straightforward extension of the above approach for the evolution of a system nucleating under time-varying supersaturation. When the supersaturation varies *continuously* as $S = S(t)$, one derives the cumulative distribution function (CDF) of nucleation probability as[17,21]

$$F(t) = 1 - e^{-\int_{t_{sat}}^{t} \kappa(s)\, ds} \tag{3}$$

in which t_{sat} is the time at which the system attains saturation (i.e., $S(t_{sat}) = 1$), and s is the dummy variable of integration. The time dependence of the rate of transition probability κ is expressed by considering $\kappa(t) = J(t)V(t)$, with the nucleation rate $J(t)$ to be given by

$$J(t) = AS(t)\, \exp\{-B/\ln^2[S(t)]\} \tag{4}$$

in which A and B are nucleation *rate parameters* (kinetic constants). Equation 4 originates from the CNT. Other equivalent or semiempirical expressions for the nucleation rate are also used in place of eq 4. The volume V of the system is a function of time $V(t)$ only if V is changing during the experiment, as in the case of evaporative crystallization. The mean time of nucleation in the system for this case is obtained as[17]

$$t_{mean} = \int_{t_{sat}}^{\infty} t\, \kappa(t)\, e^{-\int_{t_{sat}}^{t} \kappa(s)\, ds}\, dt \tag{5}$$

If the supersaturation is generated by cooling a solution with a fixed solute concentration C_0 at a constant cooling rate β, the probability distribution of ΔT (i.e., MZW) may be obtained through eqs 3 and 4 with $\Delta T(t) = \beta(t - t_{sat})$, where t_{sat} is the time at which the system temperature reaches T_{sat}. The mean temperature T_{mean} at which nucleation is expected to occur during this cooling is obtained as $T_{mean} = T_{sat} - \beta\, t_{mean}$.

2.2. New Approach to MZW. The derivation of eqs 3 and 5 intuitively extends the equality $\kappa = JV$ from the case of constant supersaturation as $\kappa(t) = J(t)V(t)$ for the case of time-varying supersaturation. However, such an extension of thought is not logical, as discussed by us previously,[21] and may lead to incorrect

DOI: 10.1021/acs.cgd.7b00875
Cryst. Growth Des. 2017, 17, 5823−5837

predictions in an MZ experiment. The new approach proposed by us to analyze the MZW experiment focuses on ΔG^*, the energy barrier to nucleation instead of the nucleation rate J. In an MZW experiment, the energy barrier is infinite at the beginning of the experiment ($S = 1$) and is lowered continuously until nucleation occurs. Here we denote the normalized energy barrier ($\Delta G^*/k_BT$) with g, where k_B is the Boltzmann's constant and T is the absolute temperature. During the gradual lowering of g in an MZW experiment, the cumulative probability of nucleation at any energy barrier g is expressed through[21]

$$F(g) = \Pr(g_n \geq g) = \int_{\infty}^{g} \exp(-g')\, dg' = -e^{-g} \tag{6}$$

The negative sign in front of the exponential in eq 6 signifies that g decreases as the experiment progresses and is of no consequence. When the supersaturation of the system varies sufficiently slowly, we may assume that at each instance the system is equilibrated to the prevailing energy barrier. In that case, within the scope of the CNT, $F(g)$ may be expressed as a function of S as[21]

$$F(S) = \exp\left(-\frac{W^* - W_1}{k_BT}\right) = \exp\left(\frac{\pi\Gamma}{3} - \frac{4\pi^3}{27}\frac{\Gamma^3}{\ln^2 S}\right) \tag{7}$$

In eq 7, W^*, and W_1 represent the reversible work of formation of a (spherical) critical cluster, and that of a cluster of 1 molecule, respectively, at S. The dimensionless solid−liquid interfacial free energy Γ is defined as $\Gamma = (\gamma d^2/k_BT)$ in which d is the solute molecular diameter and γ is the energy involved in the creation of a unit area of the new crystal surface within the solvent. The term $W_1 = (\pi\Gamma/3)$ appears in eq 7 to correct the energy barrier given by the CNT such that eq 7 satisfies the expected limiting behavior of eq 6 − that $F(g) \to 1$ as $g \to 0$.

From eq 6, one notes that the mean supersaturation ψ at which nucleation occurs in an MZW experiment corresponds to a supersaturation at which the energy barrier to nucleation drops to the level of the thermal energy (i.e., $g_{mean} = 1$ or $\Delta G^* = 1\ k_BT$).[21] In this case, $F(g_{mean}) = 1/e$, and using this result in eq 7, one may estimate this mean "induction supersaturation" ψ as

$$\psi = \exp\{\sqrt{4\pi^3\Gamma^3/(27 + 9\pi\Gamma)}\} \tag{8}$$

If the supersaturation in the experiment is generated by cooling a solution of fixed solute concentration C_0 at a constant rate β, the probability distribution of ΔT obtained experimentally may be converted to a distribution of S using eq 7, the known solubility relation $C_{eq}[T(t)]$, and the time functionality of temperature $\Delta T(t) = \beta(t - t_{sat})$. The mean temperature T_{mean} at which one expects nucleation to occur in a polythermal experiment may be obtained from the relation $\psi = C_0/C_{eq}(T_{mean})$.

3. EXPERIMENTS FROM THE LITERATURE

Experimental determination of the probability of nucleation is typically carried out by droplet (or small aliquot) experiments,[25] in which many, *presumably identical*, batches of solution (usually ≪1 mL) are subjected to the crystallization protocol simultaneously. The number of batches that produce at least one crystal, N^*, is monitored with time, and the CDF of the nucleation probability is obtained as $F(t) = N^*(t)/N$, where N is the total number of batches. While this method is typically used to determine the nucleation kinetics from induction time (IT) experiments,[26,27] a few recent studies,[19,28−30] including our own,[21] have used this method to investigate the distribution of metastable zone widths of solutes. Below we discuss the nucleation probability in the context of eq 7 applied to the reports of cooling crystallization from the literature. Two experimental protocols are considered: (i) experiments with fixed cooling rate and different solute concentrations, and (ii) experiments with fixed solute concentration but with different cooling rates.

3.1. Experiments with Fixed Cooling Rate. For this experimental protocol, we consider the data reported by Kadam et al.[19,31] on paracetamol crystallization from water, and by Nordström et al.[29] on salicylamide crystallization from methanol.

Kadam et al. have used 1 mL batches of aqueous solution of paracetamol in their study. The experiments were performed in a high-throughput solubility apparatus (Crystal16).[32] This experimental setup detects the onset of nucleation through a reduction in the light transmittance through solution. In these experiments, the concentration of paracetamol in the solutions ranged from 0.015 g/mL to 0.047 g/mL.[31] The solutions were held at ∼5 °C above their respective saturation temperatures at the beginning of each experiment and were cooled subsequently at a constant rate $\beta = 0.5$ °C/min while being stirred at 700 rpm. The observed "cloud point" (T_n) was used in conjunction with the saturation temperature (T_{sat}) obtained from the solubility data[31,33] to determine the MZW as $\Delta T = T_{sat} - T_n$. For each solute concentration, the ΔT values obtained from a statistically significant number of batches were used to construct the probability distribution as $F(\Delta T) = N^*(\Delta T)/N$, as discussed above.

The experiments by Nordström et al. we consider here were carried out with 15 mL batches of salicylamide−methanol solutions. In these experiments, a stock solution was prepared at the desired solute concentration and was dispensed into multiple vials. These vials were placed in a cryostat and the bath temperature was gradually reduced. The onset of nucleation and nucleation temperature were recorded using a camcorder. The concentration of salicylamide used in these experiments corresponded to a T_{sat} ranging from 30 to 50 °C. Solutions that were significantly above the saturation temperature were first allowed to equilibrate to T_{sat}, and were subsequently cooled at a rate $\beta =$ 0.5 °C/h. The solutions were stirred at 400 rpm using magnetic stirrers during the experiments. Distributions of MZWs as $\Delta T = T_{sat} - T_n$ were generated from the observed T_n.

3.2. Experiments with Fixed Solute Concentration. For this type of experiments, we use the data published by Kulkarni et al.[28] on the distribution of ΔT exhibited by isonicotinamide (INA) Form II crystals from ethanol, and those by Yang et al.[30] which concern the MZW of L-ascorbic acid crystallizing in water.

The work by Kulkarni et al. is also associated with the same research group as Kadam et al. discussed above and uses the above-mentioned experimental technique with Crystal16. In this study, several 1 mL batches of 102 mg/mL INA solution were cooled at different cooling rates in the range of $\beta = 0.1$−1.0 °C/min. These aliquots of solution were stirred at 700 rpm during the cool-down. The values of ΔT were determined using the solubility data obtained as a part of the work. Cumulative probability distributions $F(\Delta T)$ were then generated from the available ΔT data as $F(\Delta T) = N^*(\Delta T)/N$. Kulkarni et al. also report the results of induction time (IT) experiments on the INA−ethanol system carried out at various supersaturations using a similar experimental protocol and the same experimental setup.

Yang et al.'s experiments on L-ascorbic acid were also carried out with 1 mL batches of solution using the Crystal16 apparatus. A stock solution with a solute concentration of 0.4468 g g^{-1} of water (corresponding to a $T_{sat} = 35$ °C) was prepared and was subdivided into smaller volumes. The rate of cooling in these experiments ranged from $\beta = 3$−18 °C/h. The solutions were stirred at 1000 rpm using magnetic stir bars. The observed data on T_n were processed in a similar manner as discussed above to generate the distributions of MZW for L-ascorbic acid nucleation in water at various cooling rates.

3.3. Data Extraction and Processing. In refs 19, 28, 29, and 30, the probability distributions of ΔT obtained from the experiments were presented in the form of figures, and the raw data were not available to us for some of these data sets. The raw data on the metastable zone width of INA published in ref 28, and that on salicylamide from ref 29, were provided to us by the respective authors. For the remaining data sets, we extracted the data from the published figures using high-resolution images available from the respective journals' Web sites. These images

DOI: 10.1021/acs.cgd.7b00875
Cryst. Growth Des. 2017, 17, 5823−5837

were digitized using Engauge Digitizer (v10.0), an open-source application for data extraction. Where the data were presented as dense clusters of symbols in some of the original figures, a small inaccuracy is expected in the extracted data.

Rigorously, supersaturation is defined as the ratio of activity of the solute at a given condition to that at equilibrium. For dilute solutions, the activity coefficients, and/or their ratio, often approach unity, and supersaturation is given by the ratio C_0/C_{eq} with sufficient accuracy. Hence, in this work we calculated supersaturation as $S = C_0/C_{eq}$. Even though the experimental conditions etc. are described in terms of the original units of concentration used by the respective authors in refs 19, 28, 29, and 30, to be consistent in the definition of supersaturation S across various data sets, we used g/mL as the units for C_0 and C_{eq} in our calculations. For each data point the supersaturation of nucleation S_n was determined, and the experimental probability distributions were reconstructed as $F(\Delta T)$ and $F(S)$. All the temperatures used were in °C. The values of parameter Γ in eq 7 that best describe the reconstructed probability distributions were obtained using the standard nonlinear parameter estimation procedure implemented by the mathematical software *Mathematica* (v11.1, Wolfram Research).

3.4. Crystal Growth Time (t_g). Kadam et al. and Kulkarni et al. have proposed that the metastability of solutions in their experiments was lost by a "single nucleus mechanism".[31] Experimental observations indicated that first a single crystal may form in the solution, which subsequently undergoes attrition on contact with the stirrer (either magnetic or overhead). This attrition results in a sudden shower of crystals through secondary nucleation. Kadam et al. suggested that in their experiments the metastable zone boundary (cloud point T_n) detected by the Crystal16 apparatus corresponded to this secondary nucleation event. From the live images of crystallizing solutions, these authors noted that a single "parent" crystal may grow up to 200 μm before it contacts the agitator and undergoes attrition. To account for the time taken for a crystal to grow to ~200 μm, these authors have considered a crystal growth time t_g, by which they offset the time axis in their data analysis.

To be consistent with the analysis of these authors, we also have accounted for t_g for the data on paracetamol and isonicotinamide as described in the Supporting Information. However, as shown in the Supporting Information, we observed no significant differences in the trends of the MZW distributions in the supersaturation space (i.e., in $F(S)$) whether we employ a t_g-correction or not. The possible reasons for the effect of t_g to be not significant in the experiments by Kadam et al. and Kulkarni et al. are discussed in the Supporting Information. From this perspective, and in line with the original analysis of the other authors, we employed no t_g-correction for the data sets on salicylamide and L-ascorbic acid.

4. RESULTS

The fundamental variable that drives crystal nucleation is the chemical potential difference $\Delta\mu$ of the solute resulting from the phase transformation. $\Delta\mu$ is related to supersaturation S through the functionality $\Delta\mu = k_B T \ln(S)$. Hence, below we analyze the experimental data in terms of S and the rate of generation of driving force $d[\Delta\mu(t)/k_BT]/dt$. For the sake of brevity, hereafter we denote $d[\Delta\mu(t)/k_BT]/dt$ with r, whose value is given by $d[\ln S(t)]/dt$.

4.1. Paracetamol–Water System. First, from the known information and the procedure described in Section 3.3, we calculate the path of the experiments for the four cases of paracetamol MZW studied by Kadam et al.[19,31] – with C_0 = 0.015, 0.022, 0.032, and 0.047 g/mL. The saturation temperatures given by the authors corresponding to these C_0 values are 25.8, 38.6, 49.2, and 59.1 °C, respectively,[19] and the cooling rate used was 0.5 °C/min. Figure S1 in Supporting Information shows the evolution of $S(t)$ and $r(t)$ for these cases. We observe that while the supersaturation S continuously increases during the gradual cool down of the solutions (Figure S1a), the rate of change of driving force ($r = d[\ln S(t)]/dt$) *decreases* with time (Figure S1b). This trend of r is opposite to that followed by r in the case of evaporative crystallization.[21] Also, depending on the initial solute concentration, r may even follow a non-monotonic trend. These peculiarities highlight the aspect that a constant rate of cooling (linear temperature profile) not necessarily result in a monotonic constant rate of change of driving force.

Figure 1a shows the cumulative probability distributions $F(\Delta T)$ obtained by Kadam et al. as functions of ΔT for the four cases.[19] The distributions appear significantly different from each other, supporting the prevalent notion that the metastable zone width is a function of the path of the experiment $r(t)$. We examine this notion further by transforming these distributions into the supersaturation space. Figure 1b shows the same experimental distributions, plotted as functions of the supersaturation of nucleation S_n. We observe that the four distributions, which appear to be different in the ΔT-space, collapse into a single distribution in the S-space! This result clearly shows that nucleation in all the four cases followed the same probability distribution governed by supersaturation independent of its time-course $S(t)$, and the perceived path-dependence of the MZW as $F(\Delta T)$ is not real.

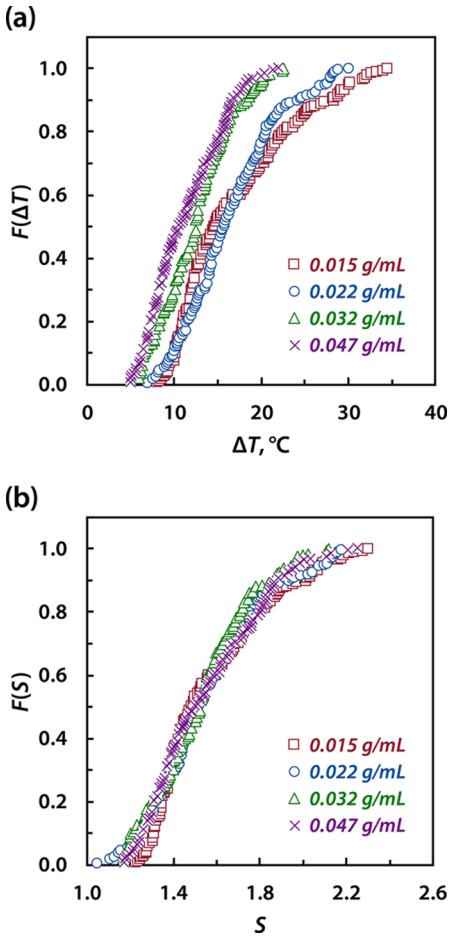

Figure 1. Cumulative probability distributions of metastable zone width for paracetamol as functions of (a) the undercooling ΔT and (b) the supersaturation S. The numbers in the figure legends indicate the solute concentration C_0 in various cases. The differences in the distributions seen in the ΔT-coordinate space are not observed in the S-coordinate space, suggesting that the MZW distribution did not depend on the experimental path for these four cases.

DOI: 10.1021/acs.cgd.7b00875
Cryst. Growth Des. 2017, 17, 5823–5837

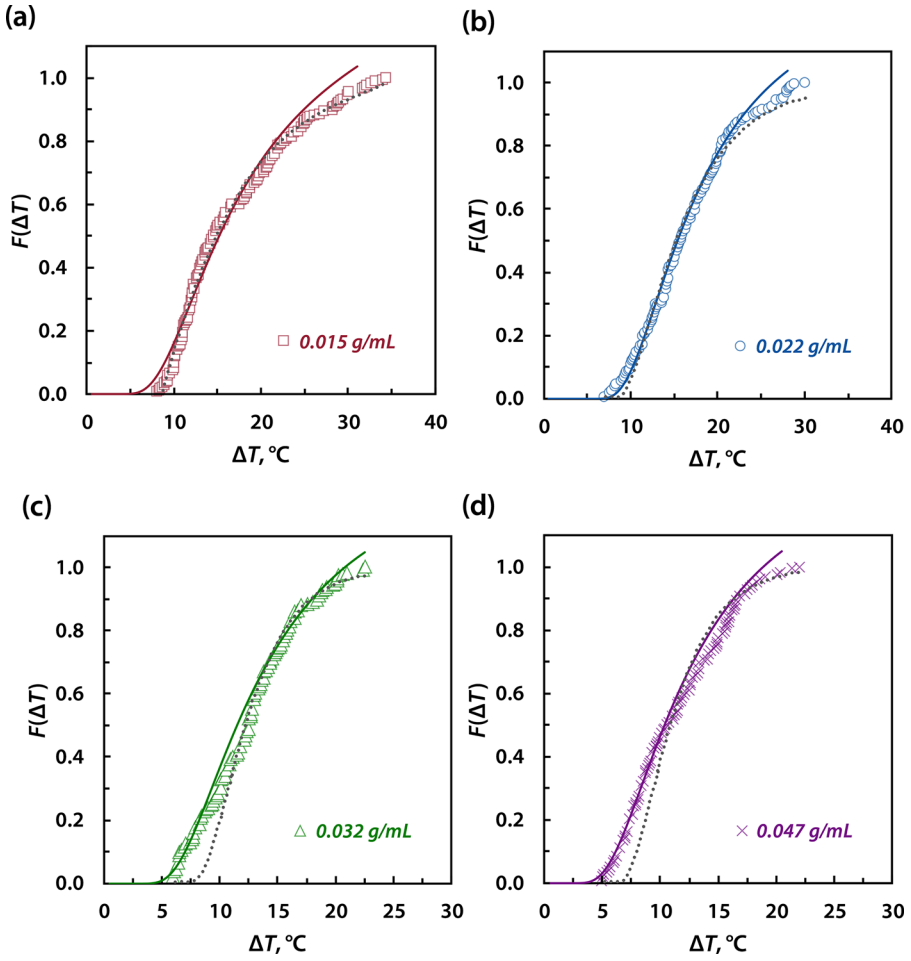

Figure 2. Comparison of model fits of eq 7 to the experimental distributions of MZWs for paracetamol for the four solute concentrations (a) 0.015 g/mL, (b) 0.022 g/mL, (c) 0.032 g/mL, and (d) 0.047 g/mL. The symbols indicate the experimental data and the solid lines are the fits to eq 7. The dotted lines indicate the fits of eq 3 as provided by Kadam et al, redrawn from ref 19. Equation 7 fits the data comparable to, if not better than, eq 3.

The result shown in Figure 1b is in line with our observations from evaporative crystallization of various solutes, including paracetamol.[21] This common, path-independent, $F(S)$ curve also indicates that the experiments on paracetamol were conducted sufficiently slowly such that the "equilibrium assumption"—the assumption that the solution is equilibrated to the imposed supersaturation at all times—holds good.

Above in Figures 2a–d we show the ability of eq 7 to describe the observed probability distributions of ΔT. For each case, we fit the experimental distributions in the supersaturation space to eq 7 and obtain the values of Γ that best describe the data. For convenience, the plots in Figure 2 present the experimental data in the observed ΔT-space. Also shown in Figure 2 with dotted lines are the fits to the conventional "rate" model, (eq 3 in combination with a variant of eq 4) as provided by Kadam et al.[19] As we observe from Figure 2, eq 7 captures the experimental distribution of MZWs very well in each case, and the fits are comparable in quality to, if not better than, those from eq 3 used by Kadam et al. Note that eq 3, as used by Kadam et al., contains three parameters—two adjustable parameters A, B, and a specified growth rate constant k_g that varies for each case—whereas eq 7 contains only one adjustable parameter, Γ, and a specified growth rate constant k_g that is the same for all of the data sets. As discussed in the Supporting Information, eq 7 describes the data equally well even if we do not account for the crystal growth time (i.e., not use k_g) in deriving the MZW distributions as $F(S)$.

Table 1. Interfacial Free Energy Parameters (Γ) for Paracetamol Obtained from Fitting the MZW Distributions in Figure 1b to eq 7[a]

solute conc. (g/mL)	Γ dimensionless	uncertainty[b] (±)	RMSE[c]	γ (mJ/m^2)
0.015	0.3415	0.0029	0.0498	3.277
0.022	0.3416	0.0025	0.0411	3.279
0.032	0.3322	0.0025	0.0391	3.189
0.047	0.3365	0.0029	0.0455	3.230

[a]Also shown are the values of specific interfacial free energy γ calculated at 25 °C. [b]The uncertainty represents the 95% confidence interval for the estimated Γ. [c]The root mean-squared error (RMSE) is determined for the fit of $F(S)$ vs S.

The values of the dimensionless interfacial free energy (Γ) obtained by curve fitting, and the error bounds on Γ for each case, are given in Table 1. We note that the Γ obtained from all the four cases is of nearly the same value. This is an expected result given the collapse of ΔT distributions into a master distribution seen in Figure 1b. The values of the specific interfacial free energy γ (calculated at 298.15 K) are also given in Table 1. These values of γ cannot be directly compared to those obtained by Kadam et al. for two reasons: (i) The theoretical arguments that underlie eq 3

DOI: 10.1021/acs.cgd.7b00875
Cryst. Growth Des. 2017, 17, 5823–5837

and eq 7 is are very different, and the parameter values obtained from curve-fitting are not comparable, (ii) in calculating γ from Γ, we used a molecular volume of 1.471×10^{-28} m^3 for paracetamol, estimated from a crystal density of 1.263 g/mL and a crystal packing fraction of 0.74 as suggested by He et al.[34] Kadam et al. report that they used a molecular volume of 1.94×10^{-26} m^3. The 2 orders of magnitude difference in the used molecular volume results in a significant difference in the calculated molecular diameter d (3.33 nm for Kadam et al.'s case vs 0.655 nm in our case) and hence to a difference in the estimated γ from the relation $\Gamma = (\gamma d^2/k_B T)$.

4.2. Salicylamide−Methanol System. For the salicylamide−methanol system studied by Nordström et al.,[29] the five MZW distributions we consider here were obtained with solutions in which C_0 corresponded to T_{sat} of 30, 35, 40, 45, and 50 °C. Figure S2 in Supporting Information shows the time course of $S(t)$ and $r(t)$ for these cases. We note that in all these cases the evolution of supersaturation with time is the same (Figure S2a). The rate of change of driving force, however, follows various nonmonotonic trends (Figure S2b). Note that the values of r are about an order of magnitude lower than those observed for paracetamol (cf. Figure S1b), and the variations in r with time appear to be insignificant.

The distributions of MZW as functions of ΔT for the five cases are shown below in Figure 3a. Figure 3b shows the same distributions in the S-coordinate space. We observe that the $F(S)$ curves in Figure 3b coincide for data sets with T_{sat} = 30, 35, and 45 °C, a result that is in line with our earlier observations with paracetamol−water system. The distributions for T_{sat} = 40 and 50 °C start with following the same master trend initially, but deviate abruptly. Given the small values of r, it is unlikely that these deviations are a result of time lags to equilibration in the systems. These abrupt changes in the slope of the MZW curves rather than a smooth variation, and the fact that these experiments used relatively large batch of solutions (15 mL) in comparison to those by Kadam et al. (1 mL), indicate that nucleation in some of these vials may have been influenced by different heterogeneities than the rest.[20] Other source of deviation may be the possible "low-boiling" solvent (methanol) evaporation at high temperatures in some experimental batches.

Figure 4a−d shows the fits of eq 7 to the observed probability distributions $F(S)$ presented in terms of ΔT. These figures show that the experimental data are described well by eq 7 for the three cases of T_{sat} = 30, 35, and 45 °C. The model fails to capture the experimental distribution obtained with T_{sat} = 45 and 50 °C. This disagreement may be attributed to the possible experimental uncertainties considered above. The values of the dimensionless interfacial free energy (Γ) obtained by curve fitting, and the error bounds on Γ for each case, are given in Table 2. As expected, Γ for the three cases of T_{sat} = 30, 35, and 45 °C is of nearly the same value. Despite the poor fit between the data and the model, Γ obtained for T_{sat} = 50 °C is also nearly equal to that for the other three cases. The values of the specific interfacial free energy γ (calculated at 298.15 K) are also given in Table 2. In calculating γ from Γ, we used a molecular volume of 1.267×10^{-28} m^3 (a molecular diameter of 0.623 nm) for salicylamide, estimated from a crystal density of 1.33 g/mL and a crystal packing fraction of 0.74 as suggested by He et al.[34]

4.3. Isonicotinamide−Ethanol System. The experimental data by Kulkarni et al.[28] on the MZW of isonicotinamide in ethanol consisted of five data sets, generated using five different cooling rates − 0.1, 0.2, 0.4, 0.5, and 1.0 °C/min. All these experiments were performed with the same solute concentration

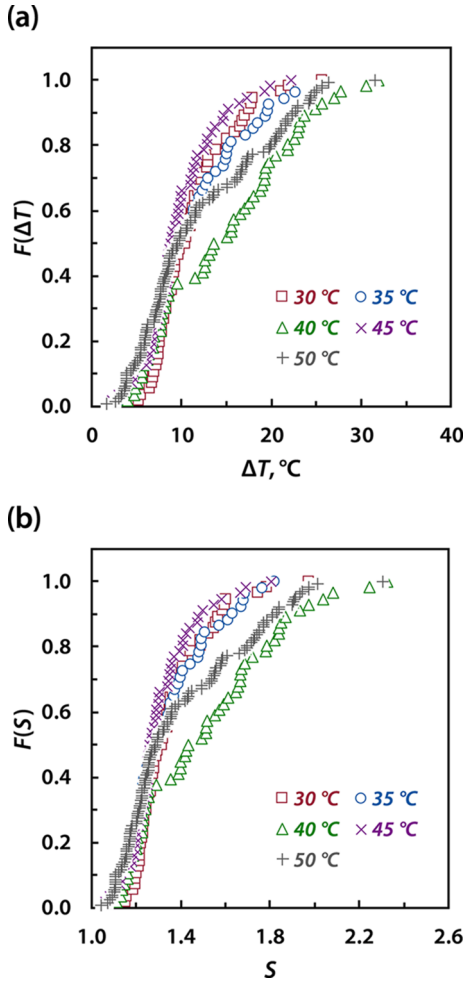

Figure 3. Cumulative probability distributions of metastable zone width for salicylamide crystals as functions of (a) the undercooling ΔT and (b) the supersaturation S. The numbers in the figure legends indicate the saturation temperatures T_{sat}. The abrupt deviations in the trends for the data with T_{sat} = 40, and 50 °C could have resulted from experimental uncertainties.

of 102 mg/mL. Reference 28 does not present the MZW distributions obtained with β = 0.2 °C/min, but these data were provided to us by the authors through personal communication. We analyze these data using a similar procedure we used for paracetamol. Figure S3 in Supporting Information shows the time evolution of supersaturation $S(t)$ and the rate of change of driving force $r(t)$ in these experiments. The changes in S and r with time are more pronounced in these cases compared to those seen in Figure S1 for paracetamol and in Figure S2 for salicylamide. Figure S3b shows that r is a nonmonotonic function of time in all these cases in the time frame considered. Larger cooling rates essentially "compress" the r-curve along the time axis.

Figure 5a−b depicts the distribution of MZWs for INA as functions of ΔT (Figure 5a) and S (Figure 5b). We observe that the distributions of MZW appear different in the ΔT-space in general as in the earlier case with paracetamol. The distributions with β = 0.1 and 0.2 °C/min overlap. When compared in S-space, these trends do not change significantly. The trends indicate that, for cooling rates ≤0.2 °C/min, the solutions may have evolved slowly enough for the "equilibrium assumption" to be valid. Under these conditions nucleation in the solutions followed the

DOI: 10.1021/acs.cgd.7b00875
Cryst. Growth Des. 2017, 17, 5823−5837

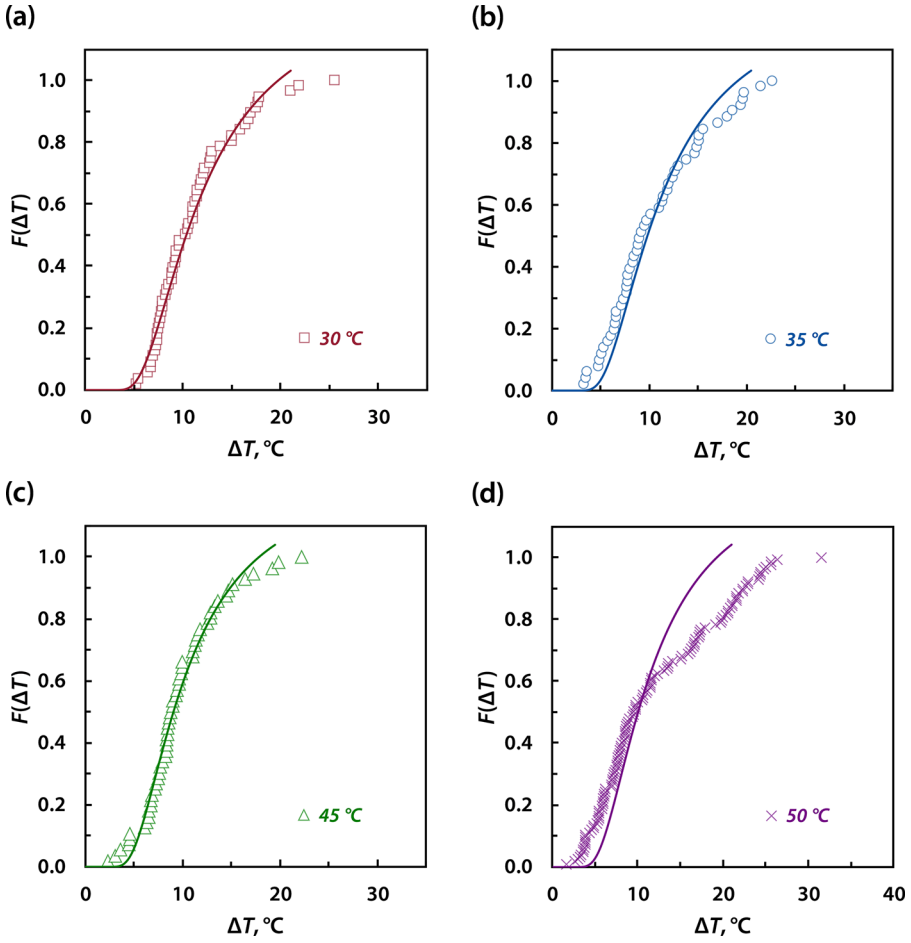

Figure 4. Comparison of model fits of eq 7 to experimental distributions of MZWs for salicylamide for the four cases of T_{sat} = (a) 30 °C, (b) 35 °C, (c) 45 °C, and (d) 50 °C. The fit for T_{sat} = 40 °C is not shown, but is comparable in quality to that with T_{sat} = 50 °C. The symbols indicate the experimental data and the solid lines are the fits to eq 7. Equation 7 describes the data well for three cases.

Table 2. Interfacial Free Energy Parameters (Γ) for Salicylamide Obtained from Fitting the MZW Distributions in Figure 3b to eq 7[a]

T_{sat} (°C)	Γ dimensionless	uncertainty[b] (±)	RMSE[c]	γ (mJ/m^2)
30	0.2488	0.0023	0.0370	2.638
35	0.2358	0.0041	0.0578	2.500
40	0.3187	0.0125	0.1287	3.378
45	0.2275	0.0023	0.0382	2.412
50	0.2448	0.0064	0.1272	2.595

[a]Also shown are the values of specific interfacial free energy γ calculated at 25 °C. [b]The uncertainty represents the 95% confidence interval for the estimated Γ. [c]The root mean-squared error (RMSE) is determined for the fit of $F(S)$ vs S.

same probability distribution in the S-space. Higher cooling rates than 0.2 °C/min may have resulted in an r high enough for the solutions to lag in equilibrating to the ever-changing supersaturation.

Figure 6a–d shows the fits of eq 7 to the data shown in Figure 5. For each case, we fit the experimental distributions in the S-space to eq 7, and regress the values of Γ that best describe the data. For comparison, these figures also show the model fits with the conventional eq 3 in combination with eq 4 as given by Kulkarni et al.[28] Since the distribution from the data with β = 0.2 °C/min practically overlaps that from the data with β = 0.1 °C/min, the model fit for this case is not shown in Figure 6. We note that in general eq 7 describes the distributions of ΔT very well. Despite the concerns about its applicability at high values of r, eq 7 still captures the observed distribution with β = 1.0 °C/min reasonably well with an effective Γ that is higher than the rest.

The values of the dimensionless interfacial free energy (Γ) obtained by curve fitting are given in Table 3. Also given in the table are the specific interfacial free energy γ calculated at 298.15 K. To calculate γ from Γ, we used a molecular volume of 1.251 × 10^{-28} m^3 for INA, estimated from a crystal density of 1.20 g/mL and a crystal packing fraction of 0.74 as suggested by He et al.[34] From Table 3, we note that the Γ obtained for β = 0.1 and 0.2 °C/min are about the same. The values of Γ progressively increase with increasing β. This result suggests that even at high r, eq 7 in form is valid and one does not need a nucleation rate to estimate the probability of nucleation. This aspect is further discussed in Section 5.5.

4.4. L-Ascorbic Acid–Water System. Let us now examine the MZW distributions of L-ascorbic acid reported recently by Yang et al.[30] These data were obtained with four different cooling rates—3.0, 6.0, 9.0, and 18.0 °C/h using aqueous solutions with C_0 = 0.4468 g/g water. Figure S4 in Supporting Information shows the time evolution of supersaturation $S(t)$ and the rate of change of driving force $r(t)$ in these experiments. As with isonicotinamide–ethanol system examined above, the changes in S and r with time are more pronounced in these experiments

DOI: 10.1021/acs.cgd.7b00875
Cryst. Growth Des. 2017, 17, 5823–5837

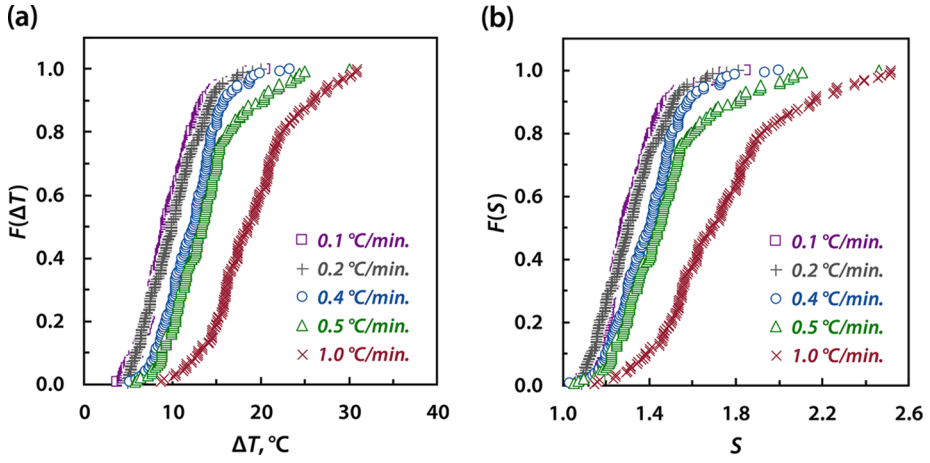

Figure 5. Cumulative probability distributions of metastable zone width for INA as functions of (a) the undercooling ΔT and (b) the supersaturation S. The numbers in the figure legends indicate the cooling rates β. The differences in the distributions seen in the ΔT-space are also present in the S-space.

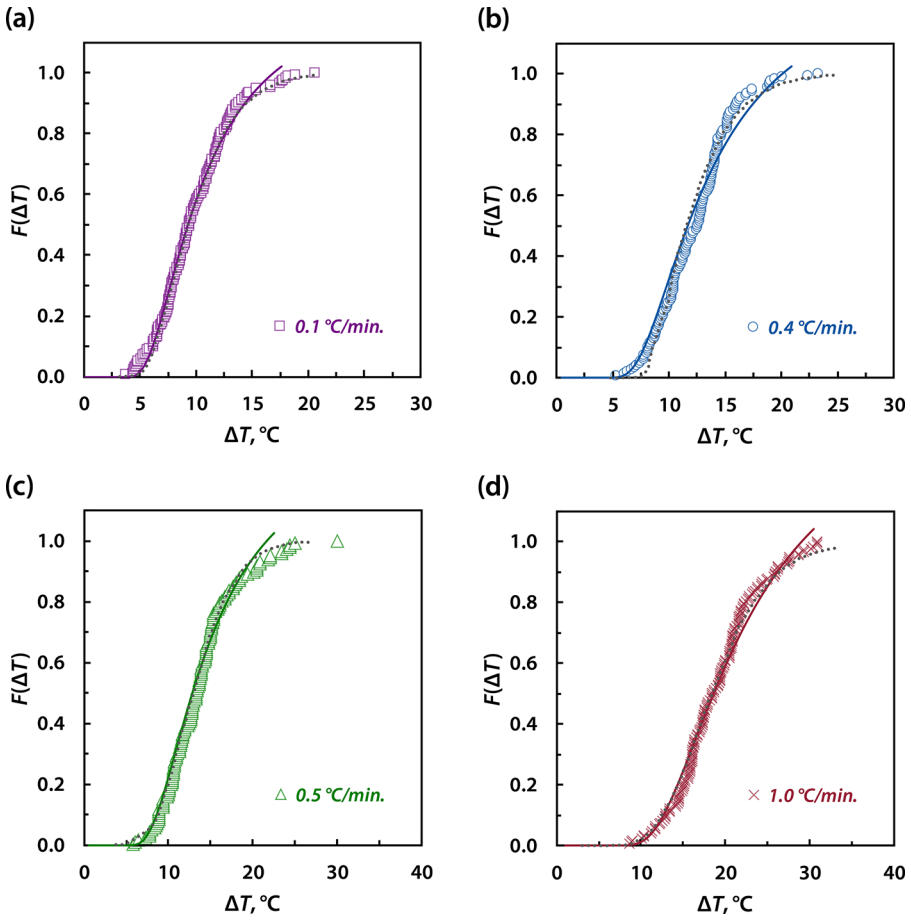

Figure 6. Comparison of fits of eq 7 to the experimental distributions of MZWs for isonicotinamide for the four cooling rates (a) 0.1 °C/min, (b) 0.4 °C/min, (c) 0.5 °C/min, and (d) 1.0 °C/min. The symbols indicate the experimental data and the solid lines are the fits to eq 7. The dotted lines indicate the fit of eq 3 as provided by Kulkarni et al, redrawn from ref 28. Equation 7 fits the data comparable to, if not better than, eq 3.

compared to those seen in Figure S1 for paracetamol and in Figure S2 for salicylamide. From Figures S1–S4, we observe that changing the cooling rate at a given solute concentration varies the path of the experiment more significantly than varying the solute concentration at a fixed low cooling rate.

In Figure 7a–b we show the distributions of MZW for this solute as functions of ΔT (Figure 7a) and S (Figure 7b). The distributions with β = 3.0, 6.0, and 9.0 °C/h are not as well-defined as the distribution obtained with β = 18.0 °C/h due to the limited number of experimental data points available to construct the curves. This lack of definition of distributions makes it difficult to clearly interpret the trends. Nevertheless, we observe that the curves with β = 3.0 and 6.0 °C/h are close to each other and partly overlap in both the ΔT-space and the S-space. Figure 8a–d shows the fits of eq 7 to the data shown in Figure 7. We note that, in general, eq 7 describes the distributions

DOI: 10.1021/acs.cgd.7b00875
Cryst. Growth Des. 2017, 17, 5823–5837

Table 3. Interfacial Free Energy Parameters (Γ) for Isonicotinamide Obtained from Fitting the MZW Distributions in Figure 5b to Equation 7[a]

cooling rate (°C/min)	Γ dimensionless	uncertainty[b] (±)	RMSE[c]	γ (mJ/m²)
0.1	0.2367	0.0008	0.0232	2.531
0.2	0.2386	0.0015	0.0422	2.551
0.4	0.2810	0.0016	0.0394	3.005
0.5	0.3022	0.0017	0.0374	3.231
1.0	0.4051	0.0015	0.0301	4.332

[a]Also shown are the values of specific interfacial free energy γ calculated at 25 °C. [b]The uncertainty represents the 95% confidence interval for the estimated Γ. [c]The root mean-squared error (RMSE) is determined for the fit of $F(S)$ vs S.

of ΔT reasonably well at cooling rates 3.0, 6.0, and 9.0 °C/h. However, in experiments with $\beta = 9.0$ and 18.0 °C/h, as observed from Figure S4b in Supporting Information and Figure 7b, the rates of change of driving force may be high enough for eq 7 to be not valid.

The values of the dimensionless interfacial free energy (Γ) obtained by curve fitting these data, and the error bounds on Γ, are given in Table 4. As expected, the values of Γ for β = 3.0 and 6.0 °C/h are close to each other. The values of the specific interfacial free energy γ (calculated at 298.15 K) are also given in Table 4. In calculating γ from Γ, we used a molecular volume of 1.3116×10^{-28} m^3 (a molecular diameter of 0.630 nm) for L-ascorbic acid, estimated from a crystal density of 1.65 g/mL and a crystal packing fraction of 0.74 as suggested by He et al.[34]

4.5. Nucleation Kinetics from IT and MZW Experiments. Induction time (IT) experiments typically focus on estimating the nucleation rate of a solute at a given supersaturation by leveraging the theoretical framework of eq 1. Extending this thought, one may consider obtaining nucleation kinetics from the MZW experiments using eq 3 (coupled with eq 4 or its equivalent) in the place of eq 1. To illustrate this approach, in ref 28, Kulkarni et al. have estimated the kinetic constants for INA (Form II) nucleation in ethanol from both the MZW experiments (using eq 3) and the induction time experiments (using eq 1). These authors provided the kinetic information obtained from both approaches as tabulated rate constants. Below we examine the nucleation rates estimated using these different experimental techniques.

Using the rate constants (A and B) given for each case in ref 28, we calculate the nucleation rate J from eq 4 in the range of S covered by the induction time experiments. This information is compared in Figure 9. The trends seen in Figure 9 are of great concern. A significant difference exists in the $J(S)$ functionality estimated from different experimental techniques. Moreover, as noted in ref 28, the MZW experiments carried out with different cooling rates resulted in conflicting rate parameter estimates. A basis for choosing any specific $J(S)$ functionality among those available is not obvious. The expected exponential trend of J with S is exhibited only by the J calculated from the IT experiments (eq 1) and from the MZW data collected with high cooling rates. The MZW experiments with low-r yielded rate information with a completely different trend.

Figure 9 suggests that the rate constants obtained from the MZW experiments are inconsistent, and this inconsistency among A and B increases as the rate of cooling decreases (i.e., in the low-r regime). Kulkarni et al. themselves have noted this possibility. These authors have concluded that, while the MZW approach in general is easy to implement, the results obtained from this approach may be of low accuracy. From the very low values of the work of nucleus formation implied by the rate constants from MZW experiments, Kulkarni et al. expressed a possibility that eq 3 may not be "accurately describing the process" of nucleation in a metastable zone. Figure 9 suggests that the kinetic information obtained from the MZW experiments may not only be of low accuracy, but also may be completely erroneous. A better approach to leverage the MZW experiments in obtaining the nucleation kinetic information is discussed below in Section 5.4.

5. DISCUSSION

Above experimental results and data analysis emphasize that, contrary to the popular notion, one does not need the information on the rate of nucleation to predict the probability of nucleation in a metastable zone. Not only the MZW may not necessarily be a path-dependent phenomenon, but also the nucleation rates estimated from the MZW measurements are likely to be incorrect and misleading. The reasons for this outcome become obvious when one considers the relation

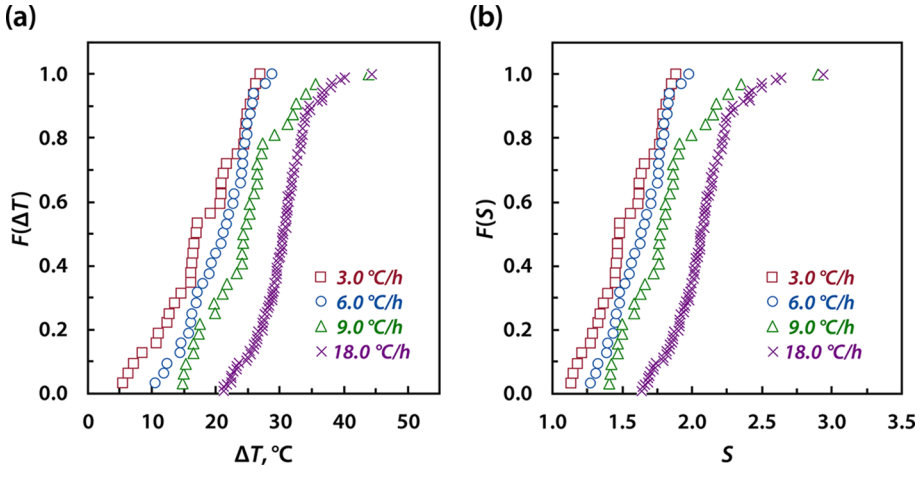

Figure 7. Cumulative probability distributions of MZW for L-ascorbic acid as functions of (a) the undercooling ΔT and (b) the supersaturation S. The numbers in the figure legends indicate the cooling rates β. The distributions seen in the S-space appear similar to those in the ΔT-space.

DOI: 10.1021/acs.cgd.7b00875
Cryst. Growth Des. 2017, 17, 5823−5837

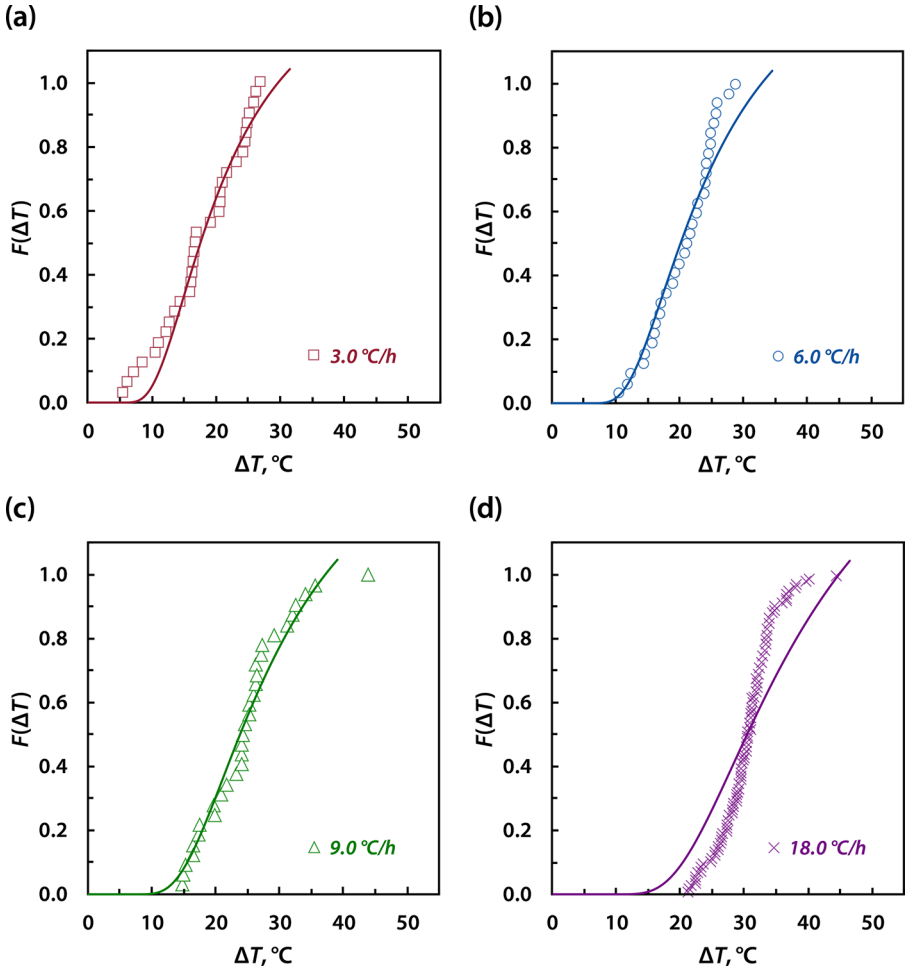

Figure 8. Comparison of model fits of eq 7 to experimental distributions of MZWs for L-ascorbic acid for the four cooling rates: (a) 3.0 °C/h, (b) 6.0 °C/h, (c) 9.0 °C/h, and (d) 18.0 °C/h. The symbols indicate the experimental data and the solid lines are the fits to eq 7.

Table 4. Interfacial Free Energy Parameters (Γ) for L-Ascorbic Acid Obtained from Fitting the MZW Distributions in Figure 7b to eq 7[a]

cooling rate (°C/h)	Γ dimensionless	uncertainty[b] (±)	RMSE[c]	γ (mJ/m²)
3.0	0.3348	0.0059	0.0523	3.468
6.0	0.3731	0.0075	0.0675	3.865
9.0	0.4258	0.0071	0.0577	4.411
18.0	0.5202	0.0097	0.1292	5.389

[a]Also shown are the values of specific interfacial free energy γ calculated at 25 °C. [b]The uncertainty represents the 95% confidence interval for the estimated Γ. [c]The root mean-squared error (RMSE) is determined for the fit of $F(S)$ vs S.

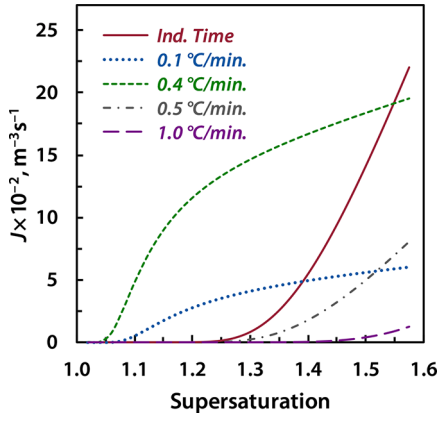

Figure 9. Trends of nucleation rate J as a function of supersaturation S for isonicotinamide. The trends are calculated from eq 4 using the kinetic constants provided by Kulkarni et al. in ref 28. The solid line indicates the J trend obtained from the induction time experiments. The various broken lines show J trends from the MZW experiments. The legend indicates the cooling rates used in the MZW experiments. The J vs S trends from the MZW experiments differ greatly from the trend obtained from the induction time experiments.

between nucleation probability and nucleation rate as defined by the Poisson view of nucleation.

5.1. Nucleation Rate and Nucleation Probability. First, let us focus on the nucleation process at a fixed supersaturation. The stochastic (Poisson) analysis of nucleation at constant supersaturation considers the system in its entirety and views a nucleation event as a rare success (critical density fluctuation) among many attempts (density fluctuations of various sizes).[21] In that sense, the rate of transition probability κ in eq 1 contains contributions from two variables: (i) the number of attempts n, and (ii) the probability of success in each attempt p. Early in the development of eq 1, one *hypothesizes* that the system tries to cross the energy barrier of nucleation with a certain attempt frequency ν, and these attempts occur *nonsimultaneously*, i.e., one after another. These assumptions allow one to express the

DOI: 10.1021/acs.cgd.7b00875
Cryst. Growth Des. 2017, 17, 5823−5837

evolution of the discrete steps of time for each attempt $(1/\nu)$ through a continuous variable t using the relation $n = \nu t$. The time-rate of change of transition probability κ is then simply given by $\kappa = p/(1/\nu) = \nu p$, allowing one to express the transition probability as a continuous function of time. Apart from this construct, within the scope of the Poisson model, there exists no theoretical basis for the required constant-κ condition.

To provide a theoretical explanation for the linearity (constant-κ) assumption, mechanistic arguments of nucleation, such as those from the classical nucleation theory (CNT),[35−37] are invoked along with statistical mechanics concepts. From statistical mechanics considerations, one expresses the probability p for the spontaneous formation of a critical cluster using the Boltzmann law as[36,38,39]

$$p = \exp(-\Delta G^*/k_B T) \tag{9}$$

in which ΔG^* is the change in the Gibbs free energy associated with the formation of a critical cluster (i.e., the energy barrier to nucleation). For a system at a fixed supersaturation S, CNT provides the steady-state nucleation rate J per unit volume of solution in the form of[36]

$$J = J_0 \exp(-\Delta G^*/k_B T) \tag{10}$$

In eq 10, the pre-exponential factor J_0 signifies the stochastic (kinetic) nature of cluster growth and the exponential term characterizes the (thermodynamic) energy barrier to nucleation.[40] CNT derives this expression for the nucleation rate J as a steady-state solution of time-evolving cluster size distribution (CSD). Hence, eq 10 indicates that, once a steady-state is achieved at a given supersaturation S, the nucleation rate J should remain constant (time-independent) at S. By equating the nucleation rate from CNT in the entire volume V to the working definition of stochastic nucleation rate κ, i.e., by considering $\kappa = JV$, one rationalizes the constant-κ assumption *ex post facto*. The Poisson attempt frequency ν now may be understood in terms of the pre-exponential factor (prefactor) J_0. Through eqs 9 and 10, one considers $\kappa = \nu p = JV = J_0 V \exp(-\Delta G^*/k_B T)$, and thus $\nu = J_0 V$. From this redefinition of variables, one now re-expresses eq 1 as

$$F(t) = 1 - e^{-JVt} \tag{11}$$

Equation 11 completes the assimilation of the stochastic perspective of nucleation into the CNT viewpoint. The probability of nucleation *at constant supersaturation* now may be characterized in terms of a more tangible nucleation rate J from a mechanistic (CNT) perspective than an elusive rate of transition probability κ.

Thus, in the original spirit of the Poisson analysis, the probability of nucleation at constant supersaturation is a function of time only through the attempt frequency ν (a hypothetical variable) and not through the nucleation rate J. The "nucleation rate" in the stochastic sense is simply a redefinition of $\kappa = \nu p$ as $\kappa = JV$ to make κ comprehensible from a CNT perspective. Note that, as discussed in Section 2.1.1, it is the distribution of t_n that *defines* (i.e., imparts physical meaning to) the nucleation rate in eq 1 and not the other way around. In principle, it may be possible to describe the distribution of t_n using a different (non-Poisson or non-Markovian) theoretical argument, in which case one need not invoke the concept of a constant rate of transition probability κ (i.e., nucleation rate). Unfortunately, such an alternate approach to explain the randomness of nucleation at a fixed supersaturation has not yet been developed due to the current limited understanding of the nucleation process.

5.2. Nucleation Probability in an MZW Experiment. In the analysis of an MZW experiment, eq 3 is derived as a straight extension of thought from eq 11 by simply interpreting the variable κ in eq 1 to be equivalent to JV. However, when one re-examines eq 3 in its original sense, as an extension of eq 1 and not of eq 11, one realizes that the $\kappa(t) = J(t)V(t)$ equivalence is questionable when S varies with time!

The underlying assumption of eq 1 is that κ should remain constant during any infinitesimal (but nonzero) time interval dt. This assumption mandates that more than one density fluctuation (attempt) should occur within dt with a frequency ν so that κ can be expressed as $\kappa = p/(1/\nu)$. This requirement is in contradiction to the condition that the supersaturation should vary continuously in an MZW experiment, which stipulates that each successive density fluctuation should occur at a different supersaturation. Thus, when S varies continuously, one cannot even define a "nucleation rate" with a physical meaning in the stochastic sense. The widely used eq 3 thus is built on assumptions inconsistent with the described physical process. Even though eq 3 appears to predict the time,[17] or temperature,[19,28] of nucleation in MZW experiments satisfactorily, it may lead to large inaccuracies in the predicted S_n. This realization led us to the development of an alternate thought process and the derivation of eq 7 in our earlier work.[21]

Equation 6 addresses these logical inconsistencies and preserves the original spirit of the Poisson description of nucleation as a rare success among many attempts. Within the scope of eq 6, the metastable zone width is only a function of the ever-changing energy barrier (g) during the experiment. Note that at high ΔT values where $F(\Delta T) \to 1$, eq 7 (derived from eq 6) overpredicts the probability of nucleation (Figures 2, 4, and 6). This is an expected behavior of eq 7, which is based on the capillarity approximation used in the CNT. At high supersaturations (i.e., large ΔT), the CNT approximation of g becomes more error-prone. Hence, eq 7 may not capture the probability of nucleation at high supersaturations where $g \to 0$. This aspect of eq 7 was discussed in more detail elsewhere.[21]

5.3. Nucleation Rates from MZW Measurements. In Section 4.3 we observed that the nucleation rates for INA crystals obtained from the induction time experiments do not agree with those estimated from the MZW experiments. This is so because within the scope of the Poisson approach, only the induction time experiments can provide reasonable estimates of the rate data. The rationale behind this statement becomes evident when one contemplates the underlying physical process described by eq 1.

Although interpreted as equivalent, the rate of transition probability κ from eq 1 and the rate of nucleation J in eq 11 have slightly different meanings. Equation 1 originates from a pure stochastic argument that is not concerned with the mechanisms of nucleation. It is designed to provide one with an *effective* nucleation rate from an experimental t_n distribution at a constant supersaturation through eq 2. This "mean" (i.e., average) nucleation rate κ does not offer any understanding of the nucleation process, but it reflects the experimental reality. The nucleation rate J from the CNT, however, claims to understand nucleation as a clustering process mediated through the attachment/detachment of *monomers*. For a given supersaturation S, J is a fixed quantity that is *not* an average, since CNT does not provide/predict a probability distribution in t_n at a fixed S.

DOI: 10.1021/acs.cgd.7b00875
Cryst. Growth Des. 2017, 17, 5823−5837

Note that eq 1 is not related to CNT. One may estimate κ directly from eq 1 using experimental data at a fixed S, thus capturing the *observed* aspects of nucleation at S. This *experimentally-real* κ may then be reinterpreted as the nucleation rate JV at S, the artificialness of CNT description notwithstanding.

When S varies *continuously*, as in an MZW experiment, no two density fluctuations (attempts) can occur with the same probability of success p. In this case, the cumulative probability of nucleation after n attempts is governed by the variation in p itself and not by the number of attempts n. Hence the construct of an attempt frequency ν to relate the number of attempts to time through $n = \nu t$ is not relevant. Without ν, the rate of transition probability κ loses its physical significance, and the premise that the change in the probability of nucleation within a time interval $(t, t + dt)$ is given by $\kappa\, dt$ is no longer physically meaningful. In other words, the concept of nucleation rate loses its relevance to describe the nucleation probability in a metastable zone. For this reason, attempts to estimate nucleation rate parameters A and B from eqs 3 and 4 by considering $\kappa(t) = J(t)V(t)$ are error-prone. The anomalies observed in Figure 7 are a direct consequence of eq 3 misrepresenting the physical process.

5.4. Complementary Nature of IT and MZW Experiments. Equation 1 only provides κ for a given supersaturation. Even in that, as discussed by Sear,[20] several experimental aspects can skew the derived values of κ from eq 1. To develop a relation between the nucleation rate J and S, one typically estimates the rate parameters A and B in eq 4 by assimilating κ within the CNT framework. This attempt usually involves fitting the $\kappa(= JV)$ values from eq 1 obtained at various S to eq 4 by considering S as a primary variable. Thus, in essence, one fitted parameter (κ) is used to further regress two more parameters A and B of eq 4. Such "double-fitting" is subject to the propagation of errors (uncertainties) in the estimated values of parameters that are hard to characterize. Moreover, exponential models such as eq 4 suffer from a significant interaction between parameters.[41,42] Mathematically, the parameters A and B estimated through eq 4 may exhibit a high degree of covariance. Often changing the initial guesses of A and B during curve fitting may converge the error-minimizing algorithms to a completely different set of estimates for A and B. To circumvent these difficulties and obtain reliable nucleation rate parameters, one may use the information provided by the MZW experiments *in combination* with IT experiments as follows. For this purpose, the nucleation rate should be defined in its stochastic form (eq 10), and not in its CNT form (eq 4), as

$$J = J_0 \exp\left(\frac{\pi\Gamma}{3} - \frac{4\pi^3}{27}\frac{\Gamma^3}{\ln^2 S}\right) \tag{12}$$

Note that in arriving at eq 12 we use eq 9 along with the equality $J = \kappa/V = \nu p/V$. In eq 12, the exponential term represents the probability of success p in a single attempt at S, and the prefactor J_0 still retains its physical meaning as the number of attempts per unit volume per unit time (ν/V).

An IT experiment effectively characterizes only the imaginary attempt frequency ν at a fixed probability of success p through eq 1. In contrast, an MZW experiment characterizes p for each attempt through eq 7. Thus, these two experimental approaches are complementary. The probability p is related to the energy barrier and the interfacial free energy through eq 9. Using the data on MZW distribution generated at a slow cooling rate, the interfacial free energy Γ for a given solute−solvent system may be estimated from eq 7.[43] Having estimated this Γ, the value of J_0 that best describes the IT data for the system may be obtained directly. For this purpose, one fits the IT distributions at various S to eq 11 with a J that is defined through eq 12. One now will have the relationships $J_0(S)$ and $p(S)$ individually derived. The sought-out relationship $J(S)$ is given by the product $J_0(S)p(S)$. This procedure allows one to estimate nucleation rate parameters J_0 and Γ one at a time from experiments that characterize each parameter independently. This procedure also helps one to avoid the mathematical artifacts in parameter estimation that arise from error propagation and strong parameter interaction. Below we illustrate this approach using the experimental data on INA obtained by Kulkarni et al.[28]

From Figure 5b, the MZW experiments on INA with a cooling rate of 0.1 °C/min appear to have been carried out in the limit of $r \to 0$. Thus, for this system, we consider Γ to be 0.2367 (Table 3). Kulkarni et al.[28] have also obtained IT distributions for the same solute at S = 1.26, 1.30, 1.36, 1.40, 1.44, and 1.48. Considering the solution volume V of 1 mL, we fit these IT data to eq 11 in combination with eq 12 and obtain the J_0 that best fits the data in each case.[44]

Table 5 lists these J_0 values obtained and the values of the nucleation rate J calculated for each supersaturation. These nucleation rates are comparable to those obtained by Kulkarni et al. using eq 1, which are also given in Table 5. Figure 10a shows these fits to the experimental data. Figure 10b shows the trend of J_0 with respect to S obtained using the procedure described above. Also shown in this figure is the general trend of the nucleation rate calculated from A and B obtained from IT data by Kulkarni et al. We note that the prefactors J_0 estimated using the stochastic approach described above track the supersaturation nonlinearly. This trend differs from the linear trend of $J_0 = AS$ used in eq 4 in the context of CNT.

Table 5. Kinetic Parameters J_0 for Isonicotinamide Crystal Nucleation in Ethanol Obtained for Various Supersaturations[a]

supersaturation (x/x^*)	$J_0 \times 10^{-2}$ m^{-3} s^{-1}	uncertainty[b] (±)	$J \times 10^{-2}$ m^{-3} s^{-1}	$J \times 10^{-2}$[c] m^{-3} s^{-1}
1.26	0.593	0.013	0.210	0.22
1.30	1.210	0.029	0.570	0.64
1.36	4.473	0.072	2.762	2.68
1.40	6.132	0.095	4.262	4.50
1.44	8.877	0.272	6.760	7.10
1.48	13.654	0.295	11.142	11.50

[a]A Γ of 0.2367 (Table 3) was used in estimating J_0 in eq 12 from induction time data fit to eq 11. Also shown are the values of nucleation rates calculated from these J_0 and Γ, and the nucleation rates reported by Kulkarni et al. [b]The uncertainty represents the (95% confidence interval) $\times 10^{-2}$ for the estimated J_0. [c]These values of J are those reported in ref 28.

5.5. Path Dependence of MZW. Polythermal experiments that determine the MZW consistently show that the rate of cooling influences the observed MZW for many solutes.[8,9] In light of these experimental reports, the coinciding trends of $F(S)$ shown in Figures 1b, 3b, and 5b may appear to be counterintuitive. However, this apparent paradox may be resolved when one focuses on the influence of the energy barrier to nucleation on the MZW, as captured by eq 6 and eq 7.

From Figure S1b (see Supporting Information), we note that the rates of change of driving force r for experiments with

DOI: 10.1021/acs.cgd.7b00875
Cryst. Growth Des. 2017, 17, 5823−5837

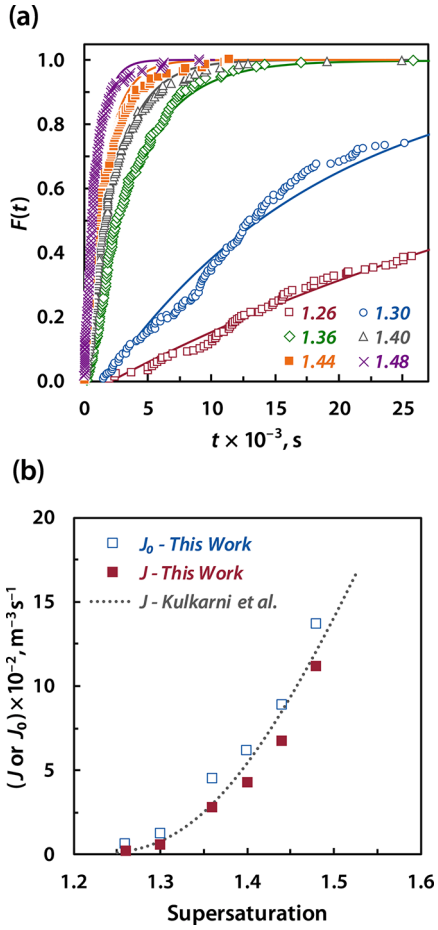

Figure 10. (a) Induction time data on isonicotinamide fit to eq 11. The symbols represent the data points and the lines are fits of eq 11 to the data using eq 12 for J with $\Gamma = 0.2367$. The numbers in the legend indicate the supersaturations at which the corresponding induction time data were obtained in ref 28. (b) The prefactors J_0 and the nucleation rates J that correspond to the model fits in panel (a). The dotted line indicates the trend of J vs S calculated using the rate constants obtained from induction time experiments by Kulkarni et al. in ref 28. The trend of J_0 vs S appears to be nonlinear in contrast to the typical linear relationship often used in the literature.

paracetamol ranged from 1.0 to 1.9 × 10^{-2} min^{-1}. These values are slightly higher than the cutoff r value of 0.4 × 10^{-2} min^{-1} (~0.25 h^{-1}) discussed for this system in our earlier work.[21] For these rates of change of driving force, we observe that all the four data sets on the MZW of paracetamol follow the same distribution of the probabilities in the S-space (Figure 1b). Since none of these distributions appear to have been influenced by r, a "critical" value of r for paracetamol above which the MZW becomes "path-dependent" cannot be established. For salicylamide, the values of r varied to a minor extent around 2.21 × 10^{-3} min^{-1}. These values are an order of magnitude lower than those for paracetamol. For this case also, we note that the MZW distributions can be collapsed into a single distribution for three of the five data sets (with only a partial overlap in the other two sets, possibly due to experimental aspects). Since r remained relatively constant in all of these experiments, a critical value of r for salicylamide, above which the MZW is influenced by the path of the experiment (i.e., $r(t)$), cannot be established.

However, for INA Form II, only distributions of MZW obtained with $\beta \leq 0.2$ °C/min are close to each other. We calculate that cooling the INA solutions at 0.2 °C/min and 0.4 °C/min should result in a maximum r of 0.6 × 10^{-2} min^{-1} and 1.3 × 10^{-2} min^{-1}, respectively (Figure S3b in Supporting Information). Thus, it appears that the "critical" rate of change of driving force for INA−ethanol system above which the lag effects become significant is in the range of 0.6−1.3 × 10^{-2} min^{-1}. For the L-ascorbic acid−water system, it is difficult to establish a critical range of r given that only a partial overlap was observed in the MZW distributions (constructed with available limited number of data points) at low cooling rates. Nevertheless, if we assume that for $\beta \leq 6.0$ °C/h the system evolves in equilibrium with changing S, a critical range of r may be estimated as 0.2 to 0.4 × 10^{-2} min^{-1} for this system (Figure S4b in Supporting Information).

These observations indicate that, in cooling crystallization, as the rate of change of driving force r (and not necessarily rate of cooling β) becomes low, the system equilibrates better to the ever-changing conditions at the molecular level, and the probability distribution of MZWs approaches a "limiting" distribution. This limiting distribution as $r \rightarrow 0$ is captured by eq 7. At higher values of r, the system lags in equilibration, and the actual energy barrier to nucleation experienced by the system at any time is higher than that calculated from the cooling rate. Hence, the probability of nucleation at any supersaturation perceived by the experimenter is lower than that in a low-r case. Thus, we resolve the paradox of the apparent path-dependence of the MZW.[21]

On a first glance, "critical" r values of the order of 10^{-3} to 10^{-2} min^{-1} for crystal nucleation may appear to indicate a lag time scale of the order of hours for equilibration. However, note that the supersaturation and the energy barrier are not linear functions of time when the experiment is performed with a constant cooling rate. The energy barrier is a function of the logarithm of supersaturation, and the supersaturation is a nonlinear function of time in this case. The probability of nucleation in turn is an exponential function of the energy barrier. Hence one may not simply estimate the lag time scales by inverting the critical range of r. A complete characterization of time scales involved in equilibration requires a rigorous "unsteady state analysis" of the problem, and such an analysis is out of the scope of the Poisson model for MZW with which this work is concerned.

6. CONCLUSIONS

The metastable zone in solution crystallization has been historically viewed as a phenomenon that originates from the path-dependence of the steady-state nucleation rate. Our recent work calls this traditional view into question. By reanalyzing the experimental data published in the literature for several solute−solvent systems, here we show that the often-reported dependence of the metastable zone width (ΔT) on the path of the experiment (i.e., on the time evolution of driving force $r(t)$) may not exist in the supersaturation space. The results shown in Figures 1, 3, 5, and 7 suggest that a comparison of MZW experiments on the basis of cooling rate alone may be misleading. These experiments may provide more useful information when the data are analyzed with a focus on the rate of change of driving force r.

The prevalent notion that the nucleation rate of crystals greatly increases at the metastable zone boundary is correct in the sense that at this boundary the probability p becomes significant due to a low energy barrier to nucleation. This increase in p leads to an increase in the nucleation rate (which is a product of p and ν).

DOI: 10.1021/acs.cgd.7b00875
Cryst. Growth Des. 2017, 17, 5823−5837

Thus, the sharp increase in the nucleation rate at the metastable zone boundary is a *result* of p becoming significant. The probability p itself does not become significant at this boundary *because* of an increased nucleation rate. In essence, p depends on the energy barrier, and the nucleation rate depends on p. This subtle distinction between the cause and effect should be noted. Thus, it is incorrect to interpret that the metastable zone width is a function of the steady-state nucleation rate, even though in effect the nucleation rate sharply increases at this MZ boundary.

The observed wide metastable zones at high cooling rates are usually rationalized through an explanation that at high rates of cooling the system spends reduced time at each intermediate supersaturation in comparison to a low rate of cooling. Upon further reflection, one realizes that this logic is incorrect. When a system is *continuously* supersaturated, the system cannot *wait* at any intermediate supersaturation. Experimental observations discussed in this work indicate that the MZW becomes path-independent at slow rates of cooling. At large rates of cooling, a path-dependence of MZW may manifest due to the lag-time effects. This path-dependence should not be attributed to the variation in the steady-state rate of nucleation along the path.

Several variables, such as the presence of foreign surfaces, impurities, and mechanical agitation, can strongly influence the outcome of an MZW experiment. Interestingly, such "unpredictable" influences of external "surfaces" on MZW have not been observed in the experiments on paracetamol-water conducted by Kadam et al. Even though these authors have used different batches of solutions and different 1 mL containers in their experiments, the resulting MZW distributions overlap consistently in the supersaturation space. This result suggests that the interfacial free energy obtained from polythermal MZW experiments may be a quantity that is typical of nucleation in large batches of solution. When opportunities for heterogeneous nucleation are minimized (e.g., in microdroplet experiments that use filtered solutions), a solute may exhibit even "wider" metastable zone width, and hence a larger estimate for Γ, than otherwise.[21]

In contrast to Kadam et al.'s experimental procedure, Kulkarni et al. have used the same solution of isonicotinamide in the same set of vials for all their MZW experiments. Despite this "consistency" in their solutions and surfaces, the nucleation rate constants obtained by Kulkarni et al. from the MZW study exhibit significant variability. However, the distributions of MZWs obtained from these experiments can be overlapped for cooling rates less than 0.2 °C (Figure 5b). These observations indicate that the inconsistency in the kinetic constants estimated from the MZW experiments arises more from the inability of eq 3 to describe the nucleation process correctly than the presumed inconsistent influence of heterogeneous surfaces. As stated by Kulkarni et al.,[28] the observed MZWs were wider and the induction times were longer when the solutions were filtered than in the case of unfiltered solutions. This effect is attributable to the removal of heterogeneous surfaces in solutions through filtration, and is consistent with one's expectations.

For reasons discussed in Section 5.3, attempts to estimate nucleation rates from the MZW experiments may yield incorrect information. This conclusion also applies to the models that consider MZW as a deterministic phenomenon.[45] A better method to obtain nucleation kinetic parameters, which leverages the complementary nature of the MZW experiments and IT experiments, is suggested in this work. The prefactors J_0 for INA Form II crystals, obtained using this method, indicate that the trend of J_0 with respect to S may be different than the linear trend typically considered by researchers (eq 4) within the context of the CNT.

Historically, the Poisson formulation of nucleation at constant supersaturation was conceived to help one deduce the ill-characterized "kinetic" parameter of nucleation (the "nucleation rate") from the experimental data. The assumptions used in the Poisson formulation were rationalized after the fact by the arguments from the CNT. The distinction between these two viewpoints (CNT and Poisson) has become blurred over time. Modern literature essentially treats the probability of nucleation as a variable governed by the nucleation rate, rather than recognizing the nucleation rate as a variable *hypothesized* to explain the experimental probability distribution of t_n *at a constant supersaturation*. This work emphasizes the need to distinguish this subtlety.

Polythermal MZW experiments typically focus on the undercooling ΔT observed for a solute as a function of the cooling rate. The results from these experiments are primarily analyzed in terms of the nucleation rate, for which various empirical expressions are used. As a result, often the emphasis on the true variables that govern nucleation, such as the rate of change of driving force, supersaturation of nucleation, is lost. Through this work, we hope to bring these fundamental variables of crystal nucleation into the forefront of the interpretation of the data from polythermal MZW experiments. This work also highlights the subtle aspects and limitations of the traditional theoretical models that describe nucleation in metastable zone.

■ ASSOCIATED CONTENT

Supporting Information

The Supporting Information is available free of charge on the ACS Publications website at DOI: 10.1021/acs.cgd.7b00875.

(i) Time evolution of supersaturation S and the rate of change of driving force r for various solutes, (ii) procedure used for determining the crystal growth rate constant (k_g), (iii) possible experimental uncertainties in assessing the effect of crystal growth time t_g on the observed MZW, (iv) MZW distributions for paracetamol and isonicotinamide in the supersaturation space without a t_g-correction for the MZW (PDF)

■ AUTHOR INFORMATION

Corresponding Author

*E-mail: vbhamidi@eastman.com.

ORCID

Venkateswarlu Bhamidi: 0000-0003-1875-0574

Paul J. A. Kenis: 0000-0001-7348-0381

Notes

The authors declare no competing financial interest.

■ ACKNOWLEDGMENTS

We are grateful to Dr. Samir Kulkarni (Pfizer) and Dr. Fredrik Nordström (Boehringer-Ingelheim) for kindly providing the raw experimental data on the MZW of isonicotinamide and salicyalmide, respectively. We express our thanks to Dr. Kulkarni, Dr. Nordström, and Prof. Herman Kramer (TU Delft, Netherlands) for previewing the manuscript. High quality graphics in this work were generated using Daniel's XL Toolbox (v 7.2.10) add-in, a free utility created for Microsoft Excel by Daniel Kraus, Würzburg, Germany.

DOI: 10.1021/acs.cgd.7b00875
Cryst. Growth Des. 2017, 17, 5823−5837

REFERENCES

(1) Thanh, N. T. K.; Maclean, N. M.; Mahiddine, S. Mechanisms of Nucleation and Growth of Nanoparticles in Solution. *Chem. Rev.* **2014**, *114*, 7610−7630.

(2) Chayen, N. E. Turning Protein Crystallisation from an Art into a Science. *Curr. Opin. Struct. Biol.* **2004**, *14*, 577−583.

(3) Blundell, T. L.; Jhoti, H.; Abell, C. High-throughput Crystallography for Lead Discovery in Drug Design. *Nat. Rev. Drug Discovery* **2002**, *1*, 45−54.

(4) Tung, H.-H.; Paul, E. L.; Midler, M.; McCauley, J. A. *Crystallization of Organic Compounds: An Industrial Perspective*, 1st ed.; John Wiley & Sons: Hoboken, USA, 2009.

(5) Schwartz, A. M.; Myerson, A. S., Solutions and Solution Properties. in *Handbook of Industrial Crystallization*, 2nd ed.; Myerson, A. S., Ed.; Butterworth-Heinemann: Woburn, 2002, pp. 1−31.

(6) Lewis, A.; Seckler, M.; Kramer, H.; van Rosmalen, G. *Industrial Crystallization: Fundamentals and Applications*, 1st ed.; Cambridge University Press: Cambridge, 2015.

(7) Nývlt, J.; Söhnel, O.; Matuchová, M.; Broul, M. *The Kinetics of Industrial Crystallization*, 1st ed.; Elsevier: Amsterdam, Netherlands, 1985.

(8) Bonnin-Paris, J.; Bostyn, S.; Havet, J.-L.; Fauduet, H. Determination of the Metastable Zone Width of Glycine Aqueous Solutions for Batch Crystallizations. *Chem. Eng. Commun.* **2011**, *198*, 1004−1017.

(9) Sahin, O.; Dolas, H.; Demir, H. Determination of Nucleation Kinetics of Potassium Tetraborate Tetrahydrate. *Cryst. Res. Technol.* **2007**, *42*, 766−772.

(10) Nývlt, J. Kinetics of Nucleation in Solutions. *J. Cryst. Growth* **1968**, *3*−*4*, 377−383.

(11) Mersmann, A.; Bartosch, K. How to Predict the Metastable Zone Width. *J. Cryst. Growth* **1998**, *183*, 240−250.

(12) Kim, K.-J.; Mersmann, A. Estimation of Metastable Zone Width in Different Nucleation Processes. *Chem. Eng. Sci.* **2001**, *56*, 2315−2324.

(13) Sangwal, K. Novel Approach to Analyze Metastable Zone Width Determined by the Polythermal Method: Physical Interpretation of Various Parameters. *Cryst. Growth Des.* **2009**, *9*, 942−950.

(14) Sangwal, K. A Novel Self-Consistent Nývlt-like Equation for Metastable Zone Width Determined by the Polythermal Method. *Cryst. Res. Technol.* **2009**, *44*, 231−247.

(15) Kashchiev, D.; Borissova, A.; Hammond, R. B.; Roberts, K. J. Effect of Cooling Rate on the Critical Undercooling for Crystallization. *J. Cryst. Growth* **2010**, *312*, 698−704.

(16) Kashchiev, D.; Firoozabadi, A. Kinetics of the Initial Stage of Isothermal Gas Phase Formation. *J. Chem. Phys.* **1993**, *98*, 4690−4699.

(17) Goh, L.; Chen, K.; Bhamidi, V.; He, G.; Kee, N. C. S.; Kenis, P. J. A.; Zukoski, C. F.; Braatz, R. D. A Stochastic Model for Nucleation Kinetics Determination in Droplet-Based Microfluidic Systems. *Cryst. Growth Des.* **2010**, *10*, 2515−2521.

(18) Peters, B. Supersaturation Rates and Schedules: Nucleation Kinetics from Isothermal Metastable Zone Widths. *J. Cryst. Growth* **2011**, *317*, 79−83.

(19) Kadam, S. S.; Kulkarni, S. A.; Coloma Ribera, R. C.; Stankiewicz, A. I.; ter Horst, J. H.; Kramer, H. J. M. A New View on the Metastable Zone Width During Cooling Crystallization. *Chem. Eng. Sci.* **2012**, *72*, 10−19.

(20) Sear, R. P. Quantitative Studies of Crystal Nucleation at Constant Supersaturation: Experimental Data and Models. *CrystEngComm* **2014**, *16*, 6506−6522.

(21) Bhamidi, V.; Kenis, P. J. A.; Zukoski, C. F. Probability of Nucleation in a Metastable Zone: Induction Supersaturation and Implications. *Cryst. Growth Des.* **2017**, *17*, 1132−1145.

(22) Toschev, S.; Milchev, A.; Stoyanov, S. On Some Probabilistic Aspects of the Nucleation Process. *J. Cryst. Growth* **1972**, *13/14*, 123−127.

(23) Van Kampen, N. G. *Stochastic Processes in Physics and Chemistry*, 3rd ed.; Elsevier: Amsterdam, The Netherlands, 2007.

(24) Bigg, E. K. The Supercooling of Water. *Proc. Phys. Soc., London, Sect. B* **1953**, *66*, 688.

(25) Turnbull, D. Kinetics of Solidification of Supercooled Liquid Mercury Droplets. *J. Chem. Phys.* **1952**, *20*, 411−424.

(26) Laval, P.; Crombez, A.; Salmon, J.-B. Microfluidic Droplet Method for Nucleation Kinetics Measurements. *Langmuir* **2009**, *25*, 1836−1841.

(27) Jiang, S.; ter Horst, J. H. Crystal Nucleation Rates from Probability Distributions of Induction Times. *Cryst. Growth Des.* **2011**, *11*, 256−261.

(28) Kulkarni, S. A.; Kadam, S. S.; Meekes, H.; Stankiewicz, A. I.; ter Horst, J. H. Crystal Nucleation Kinetics from Induction Times and Metastable Zone Widths. *Cryst. Growth Des.* **2013**, *13*, 2435−2440.

(29) Nordström, F. L.; Svärd, M.; Rasmuson, Å. C. Primary Nucleation of Salicylamide: the Influence of Process Conditions and Solvent on the Metastable Zone Width. *CrystEngComm* **2013**, *15*, 7285−7297.

(30) Yang, H.; Florence, A. J. Relating Induction Time and Metastable Zone Width. *CrystEngComm* **2017**, *19*, 3966−3978.

(31) Kadam, S. S.; Kramer, H. J. M.; ter Horst, J. H. Combination of a Single Primary Nucleation Event and Secondary Nucleation in Crystallization Processes. *Cryst. Growth Des.* **2011**, *11*, 1271−1277.

(32) Crystal16®. https://www.crystallizationsystems.com/crystal16 (4/30/2017).

(33) Grant, D. J. W.; Mehdizadeh, M.; Chow, A. H.-L.; Fairbrother, J. E. Non-linear van't Hoff Solubility-Temperature Plots and Their Pharmaceutical Interpretation. *Int. J. Pharm.* **1984**, *18*, 25−38.

(34) He, G.; Tan, R. B. H.; Kenis, P. J. A.; Zukoski, C. F. Generalized Phase Behavior of Small Molecules and Nanoparticles. *J. Phys. Chem. B* **2007**, *111*, 12494−12499.

(35) Debenedetti, P. G. *Metastable Liquids: Concepts and Principles*, 1st ed.; Princeton University Press: Princeton, USA, 1996.

(36) Kashchiev, D. *Nucleation: Basic Theory with Applications*, 1st ed.; Butterworth-Heinemann: Boston, USA, 2000.

(37) Kalikmanov, V. I. *Nucleation Theory*, 1st ed.; Springer: New York, USA, 2013.

(38) ten Wolde, P. R.; Frenkel, D. Enhancement of Protein Crystal Nucleation by Critical Density Fluctuations. *Science* **1997**, *277*, 1975−1978.

(39) Ford, I. J. Statistical Mechanics of Nucleation: A Review. *Proc. Instn Mech. Eng.* **2004**, *218* (PartC), 883−899.

(40) In eq 4, the dependence of J_0 on supersaturation, as obtained by the CNT theoretical development, is considered explicitly.

(41) Himmelblau, D. M. *Process Analysis by Statistical Methods*, 1st ed.; John Wiley & Sons: New York, USA, 1970.

(42) Bhamidi, V.; Varanasi, S.; Schall, C. A. Measurement and Modeling of Protein Crystal Nucleation Kinetics. *Cryst. Growth Des.* **2002**, *2*, 395−400.

(43) Alternately, one may conduct a few MZW experiments at very low rates of cooling, assume the observed average of S_n to be the "induction supersaturation" ψ, and obtain Γ from eq 8.

(44) Kulkarni et al. have defined their supersaturation as the ratio of mole fractions ($S = x/x^*$). We convert these values of S to conform to our definition of supersaturation as the ratio of concentrations ($S = C/C^*$) in these calculations.

(45) Sangwal, K. Recent Developments in Understanding of the Metastable Zone Width of Different Solute-Solvent Systems. *J. Cryst. Growth* **2011**, *318*, 103−109.

DOI: 10.1021/acs.cgd.7b00875
Cryst. Growth Des. 2017, 17, 5823−5837